MNRAS **000**, 000–000 (0000) Preprint 1 November 2017 Compiled using MNRAS LATEX style file v3.0

What is confining the proplyd bow shocks in Orion?

Jorge A. Tarango Yong & William J. Henney
Instituto de Radioastronomía y Astrofísica, Universidad Nacional Autónoma de México, Apartado Postal 3-72, 58090 Morelia, Michoacán, México

1 November 2017

ABSTRACT
We analyze the projected shapes of bowshocks associated with photoevaporating disks (proplyds) in the inner Orion Nebula. We show that the photoevaporation flows must be anisotropic in order to reproduce the observed shapes. The stagnation pressures of the shocked shells within 0.02 pc of the dominant high-mass star are consistent with an interaction with its unshocked stellar wind, but the more distant shells require a confining pressure that is an order of magnitude higher than can be provided by the unmodified wind. We show that these outer objects may be proplyds that are interacting with the conical wake generated by the wind-wind interaction in the inner proplyds.

1 INTRODUCTION

Proplyds are comet-like structures observed in HII regions like Orion Nebula Cluster (ONC). These objects are interpreted as a D-type Ionization Front (IF) of a photoevaporated flow originated in the protoplanetary disk of a nearby low mass YSO (Johnstone et al. 1998). The pressure of the surrounding gas is not enough to confine this flow (Henney & Arthur 1998) may be formed by the interaction of the photoevaporated wind of the proplyds with the stellar wind of θ^1 Ori C, which is highly supersonic ($M \sim 100$).

2 APPLICATION TO PROPLYD BOWSHOCKS

The density distribution of the photoevaporated flow can be determined using the steady state continuity equation and assuming that almost all ionizing photons are absorbed at the IF (Henney & Arthur 1998) and ignoring dust absorption, can be found that

$$N(r_{IF}, \theta) = N_0 \cos^{0.5} \theta \tag{1}$$

Neverthless, we should not restrict to the 0.5 index in equation (1). We may generalize this relation as follows:

$$n(r_{IF}, \theta) = n_0 \cos^{k} \theta \tag{2}$$

Where $k > 0$ implies that the wind's density decays towards wings, when $k < 0$ the wind's density incresases towards the wings and $k = 0$ implies that the wind is isotropic. In this generalization we are assuming that the inner wind is hemispheric, i.e. the density of the photoevaporated flow behind the source is zero, since equation (2) leads to non realistic values for density when $\theta > \frac{\pi}{2}$

2.1 Observational data

We measured the Characteristic radii in Orion Nebula proplyds from observations with the WPC2 camera from the Hubble Space Telescope (HST) using the narrow [OIII] filter. The original proposal were done by John Bally (The proposal ID is 5469). In figure 2, we show the field where our proplyds sample lies with the measurements of each bow shock shape we made.

2.2 Methodology

Using the DS9 SAO image tools, we marked the positions of the proplyds and θ^1 Ori C. For the shell's position, the marks were placed in the outer border of each shock. The number of marks used in each shell varies with shell's size, and with our confidence with our measurements. Thus, we used few points in small bow shocks and/our the bow shock's outer shell is not well defined. The distance D is measured as the distance between the position of θ^1 Ori C and each proplyd's position. The radius of curvature R_c is measured as the radius of the best circle fit of all the data points taken for each proplyd's shell. Finally, we measure R_0 as the distance between the proplyd's position and the circle's border in the line which include the center of curvature. To estimate the uncertainties of our measurements, we remove a fraction of the shell's marks, and made 10 sets of randomly chosen removed marks, and made the measurements again to see how much these subsamples deviates from the original data. Some examples are shown in figure (3). In the left side, for each source, the fit is done using all the shell points, while in the middle and the right we show two variations removing 2/3 of the points, but always keeping at least four. In the better observed shells such as 177-341 (top row), the circle fits are relatively robust to removing points, resulting in little variation between the subsamples. But also there are cases where the variations between subsamples are more noticeable. Colums 3, 4 and 5 of table (1) represent the summary of all the measurements done. In colums 4 and 5, the radii (R_0, R_c) are measured as the average of all subsamples, and the uncertainty as the standard deviation.

3 RESULTS

In figure (4) we show the theoretical conic curves. Most of the proplyds fit well with a elliptic-like conic shape and moderate to high degree of anisotropy of their wind.

Beneath the error margins, our measurements are consistent with Robberto et al. (2005) for R'_0/D. From figure (4), we also note that the LV4 measurements fits better with models where its photoevaporated flow is isotropic. The same is true with Robberto et al. (2005) data. The rest of the proplyds fit better with more

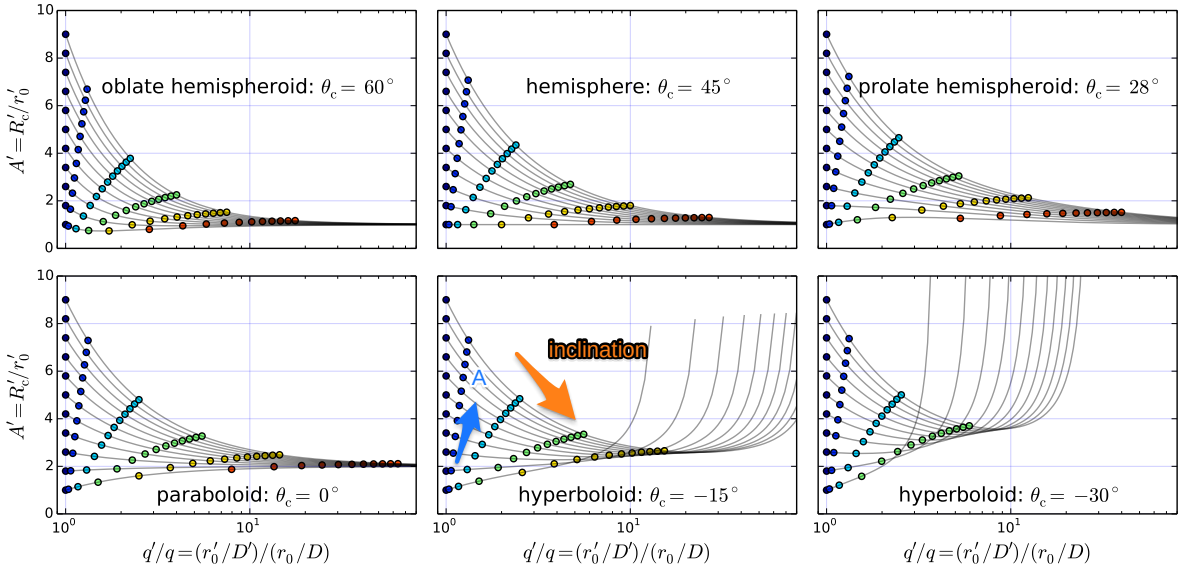

Figure 1. *Moved here from the other paper, but we probably want to get rid of it completely at some point.* Projected Radius of curvature vs projected R_0 for $\theta_c = 60°, 45°, 28°, 0°, -15°, -30°$. Each colored points represent the same shape at a different inclination. Being the dark blue the ones with the lower inclination and the red ones with the highest value. For closed shapes, there is an asymptotic limit for the projected radius of curvature at high inclinations, while for open shapes there is an upper limit for inclination where a tangent line can be observed.

anisotropic winds, which may explain why Robberto et al. (2005) did not find a match between models and data, since they only showed models where the interacting winds are isotropic.

With the data from figure 4, we derived a set of models which assumes a given set of bow shock parameters (β, i, ξ) which have agreement with the measurements of each proplyd. A given model predicts the non projected distance D for the proplyd and the non projected radius R_0. We summarize the results of the models in table 1.

From this models also we can estimate the stellar ionizing flux required to have ionization balance with the photoevaporated flow. To do this estimation we used the ionization front radius and the photoevaporated flow density measured in Henney & Arthur (1998) for each proplyd and incorporated them into the models. The result is shown in figure 5 at top. We highlight the models which have agreement with ionization balance. Also we can estimate the stagnation pressure of the photoevaporated flow. The result is shown in figure 5 at bottom. From this figures we can see that our models predict that for the farthest proplyds (169-338, 177-341 and 180-331) the stellar wind pressure is weaker than the estimated stagnation pressure. Since these bow shocks are stationary, we expect pressure balance, so the stellar wind is not enough to guarantee pressure balance far from θ^1 Ori C

4 CONCLUSIONS

Evidence for the leaky sieve model for channeling the stellar wind momentum.

Alternative would be nebular champagne flow from Orion S. We need to work out the numbers for that. But the orientation seems too close to radial for that to be plausible.

We also need to show that radiation pressure cannot be important.

Make sure we analyse the distribution of inclinations, taking into account there is a maximum inclination above which a bowshock will not be seen.

REFERENCES

Henney W. J., Arthur S. J., 1998, AJ, 116, 322
Johnstone D., Hollenbach D., Bally J., 1998, ApJ, 499, 758
O'Dell C. R., Wen Z., 1994, ApJ, 436, 194
Robberto M., et al., 2005, AJ, 129, 1534

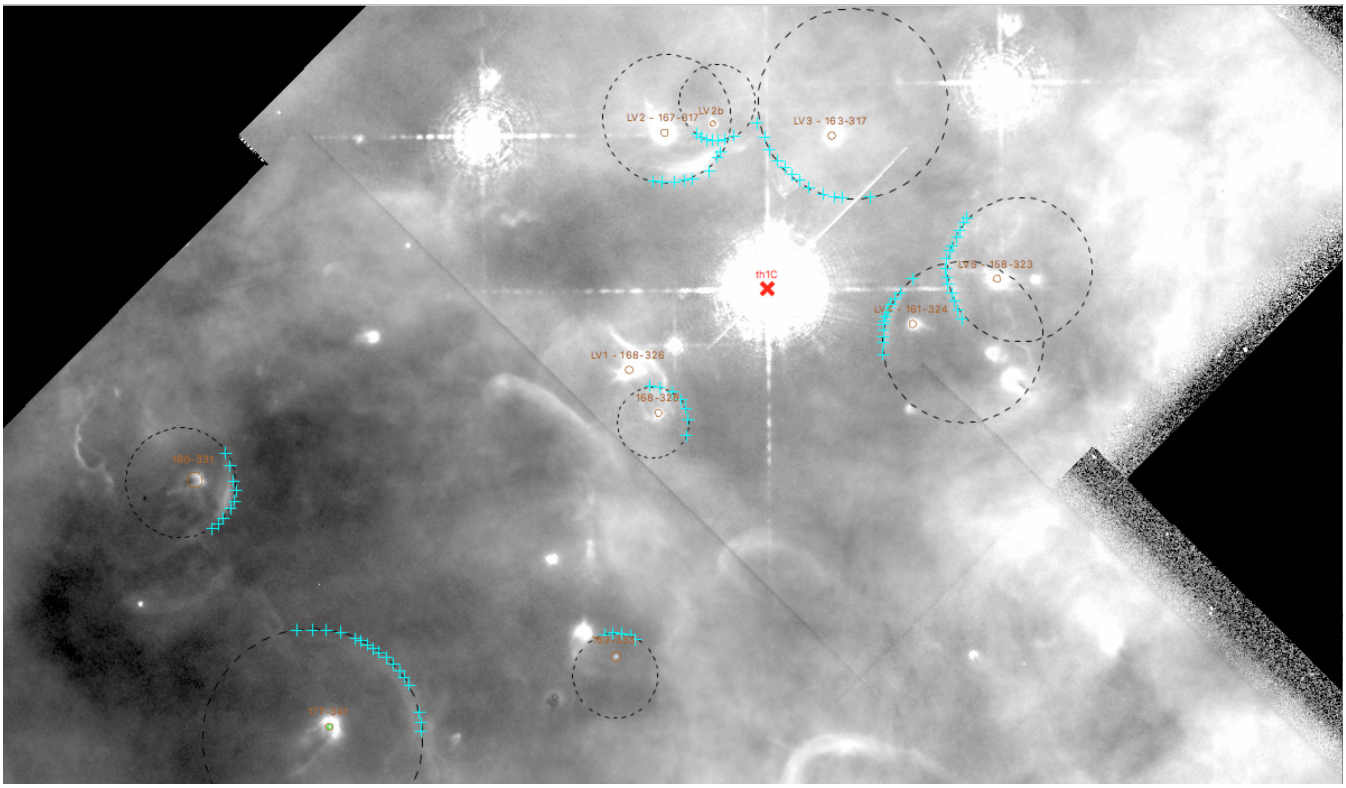

Figure 2. DS9 shell marks over ONC. The circles mark each proplys position, while the cyan crosses delineate each bow shock and the red X marks the position of $\theta^1\ C\ Ori$. The black circles only schematize a circle fit to each shell but they actually are not the real measurements.

Table 1. Fitted arc parameters for proplyd bowshocks

		Observed			Model fits					
OW	Name	D'	R'_0/D'	$(R'_c/R'_0)_{\rm shape}$	$(R'_c/R'_0)_{\rm flux}$	β	ξ	$\lvert i\rvert$	D	R_0/D
(1)	(2)	(3)	(4)	(5)	(6)	(7)	(8)	(9)	(10)	(11)
168-328		6.8	0.152 ± 0.001	1.42 ± 0.09	1.45 ± 0.05	0.018 ± 0.003	0.4 – 0.6	33 ± 3	0.017 ± 0.001	0.115 ± 0.005
169-338		16.4	0.059 ± 0.001	1.76 ± 0.48	1.50 ± 0.05	0.002 ± 0.001	0.8 – 0.8	43 ± 8	0.049 ± 0.006	0.035 ± 0.005
177-341	HST1	25.6	0.144 ± 0.001	1.21 ± 0.02	1.25 ± 0.02	0.018 ± 0.003	0.1 – 0.2	30 ± 5	0.064 ± 0.003	0.115 ± 0.005
180-331		25.1	0.061 ± 0.007	1.30 ± 0.05	1.27 ± 0.05	0.003 ± 0.001	0.4 – 0.4	35 ± 7	0.066 ± 0.007	0.047 ± 0.005
167-317	LV2	7.8	0.305 ± 0.025	0.81 ± 0.28	1.50 ± 0.1	0.085 ± 0.015	0.1 – 0.2	13 ± 13	0.017 ± 0.001	0.225 ± 0.005
	LV2b	7.2	0.097 ± 0.002	2.00 ± 0.62	1.63 ± 0.08	0.008 ± 0.003	0.8 – 0.8	28 ± 13	0.018 ± 0.002	0.078 ± 0.013
163-317	LV3	6.9	0.334 ± 0.002	1.81 ± 0.12	1.85 ± 0.15	0.075 ± 0.025	0.6 – 0.8	35 ± 5	0.018 ± 0.001	0.205 ± 0.025
161-324	LV4	6.2	0.186 ± 0.002	2.59 ± 0.24	2.05 ± 0.07	0.040 ± 0.014	0.8 – 1.0	18 ± 12	0.014 ± 0.001	0.160 ± 0.028
168-323	LV5	9.6	0.213 ± 0.002	1.57 ± 0.07	1.60 ± 0.07	0.055 ± 0.005	0.2 – 0.4	20 ± 5	0.022 ± 0.001	0.190 ± 0.010

Notes – Col. (1): Source ID (O'Dell & Wen 1994). Col. (2): Alternative name of source. Col. (3): Projected distance from θ^1 Ori C, arcseconds. Col. (4): Apparent shell outer radius along axis, normalized to projected distance, with $\pm 1\sigma$ uncertainties, determined from circle fits described in § 2.2. Col. (5): Apparent shell radius of curvature, normalized to radius along axis, with $\pm 1\sigma$ uncertainties, determined from circle fits described in § 2.2. Col. (6): As Col. (5) but applying the additional requirement that the proplyd surface brightness from model fits should agree with the theoretical prediction. Col. (7): Proplyd-to-O star wind momentum ratio (see § **??**). Col. (8): Proplyd wind anisotropy factor. Col. (9): Inclination to plane of sky, degrees. Col. (10): True distance from θ^1 Ori C, parsecs. Col. (11): True shell radius along axis, normalized to distance.

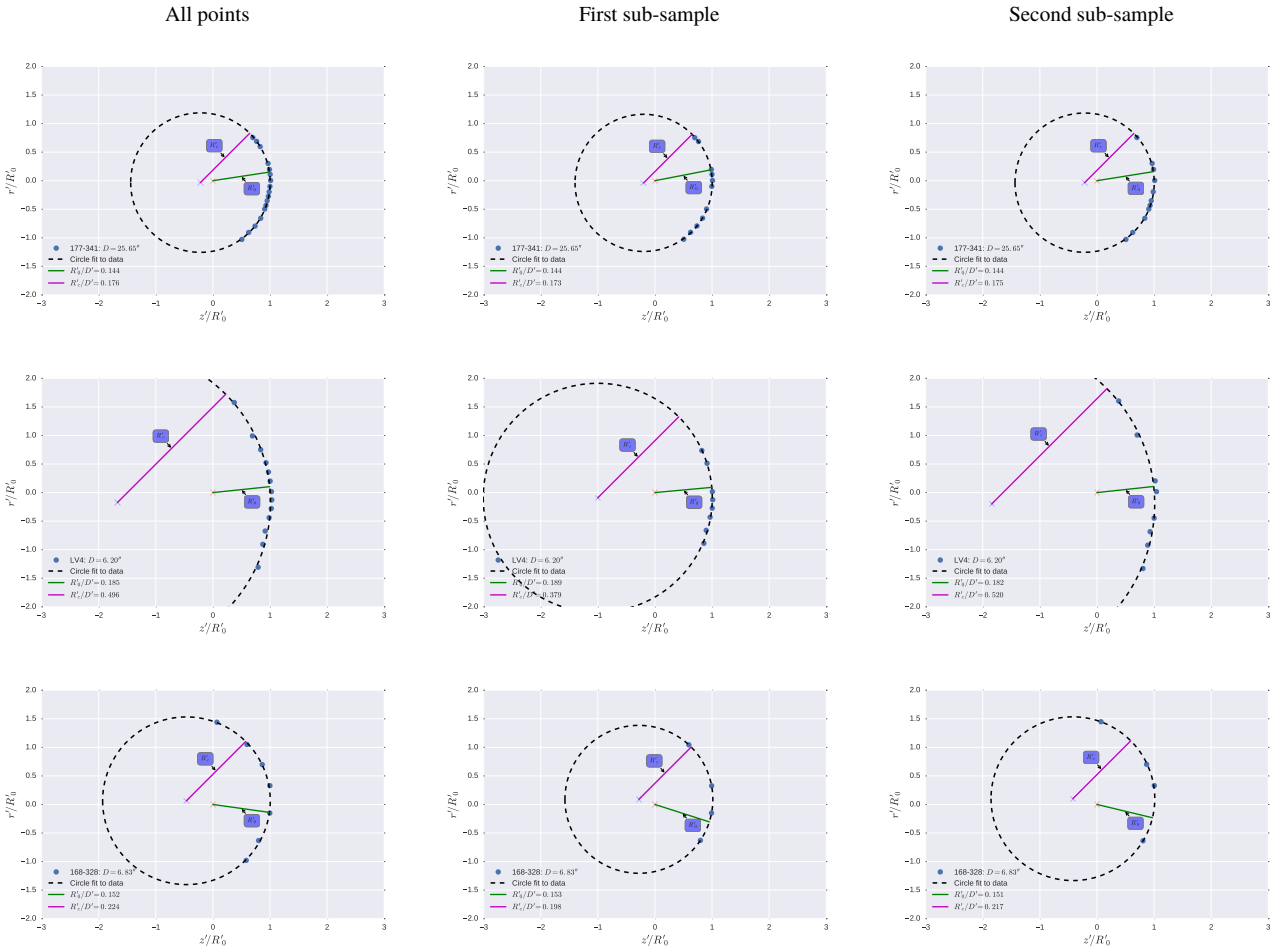

Figure 3. Examples of systematic uncertainties in the circle fits to the shell shapes for three sources (top to bottom rows): 177-341, LV4 and 168-328. The left hand column shows the fit to all of the points identified on the shell border, where the number and spacing of the points is a subjective measure of our confidence in tracing the edge of each shell. The remaining two columns show fits to randomly selected sub-samples of 2/3 of the points for each shell.

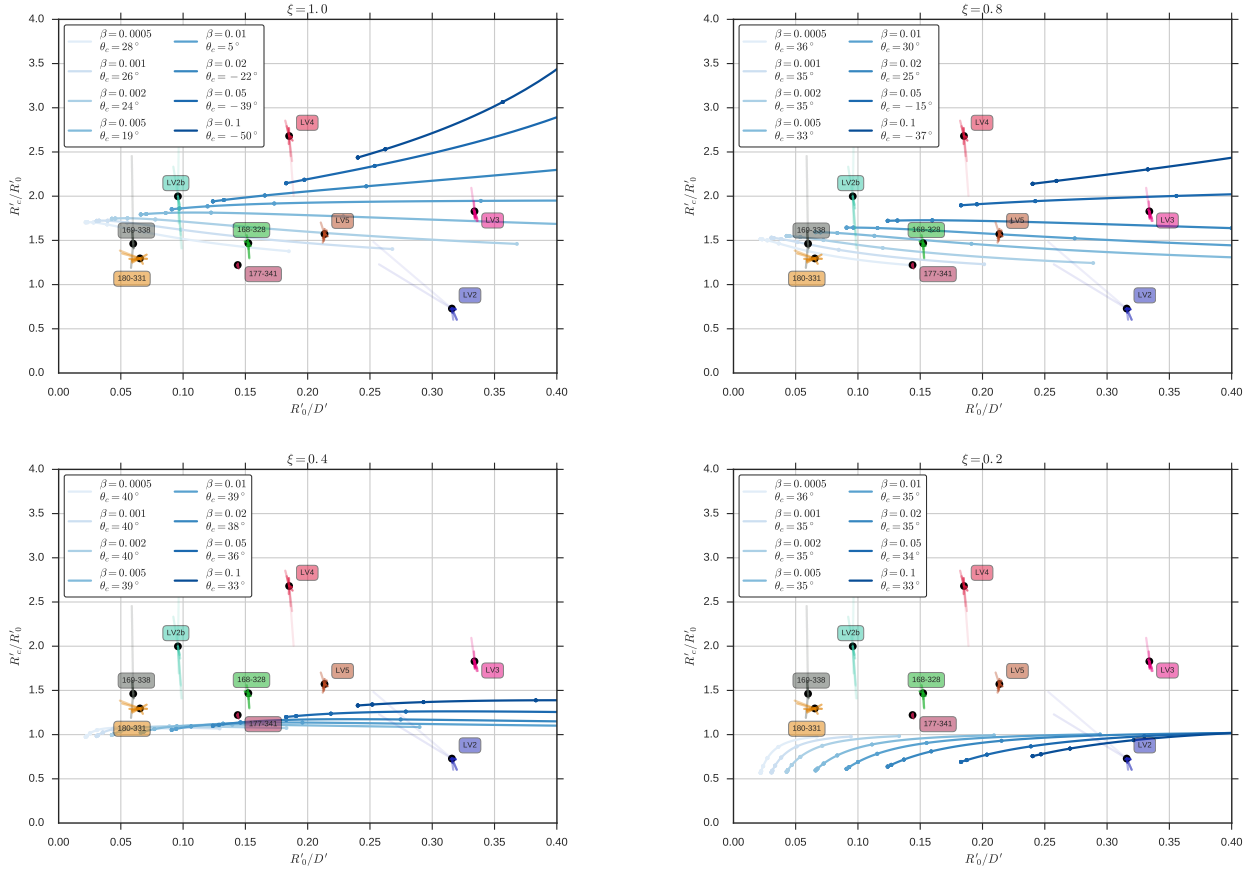

Figure 4. Measurements of proplyd's characteristic radii R_c and R_0. The curves represent a conic-like bow shock with fixed momentum ratio β and the derived value of θ_c is also shown.The dots along each curve represent separation in inclination of 15°. The measurements of each proplyd are accompained with the set of variations represented as colored radial lines. In each graph we use a different degree of the weaker wind anisotropy, starting from an isotropic wind ($\xi = 1$), to the most anisotropic wind ($\xi = 0.2$).

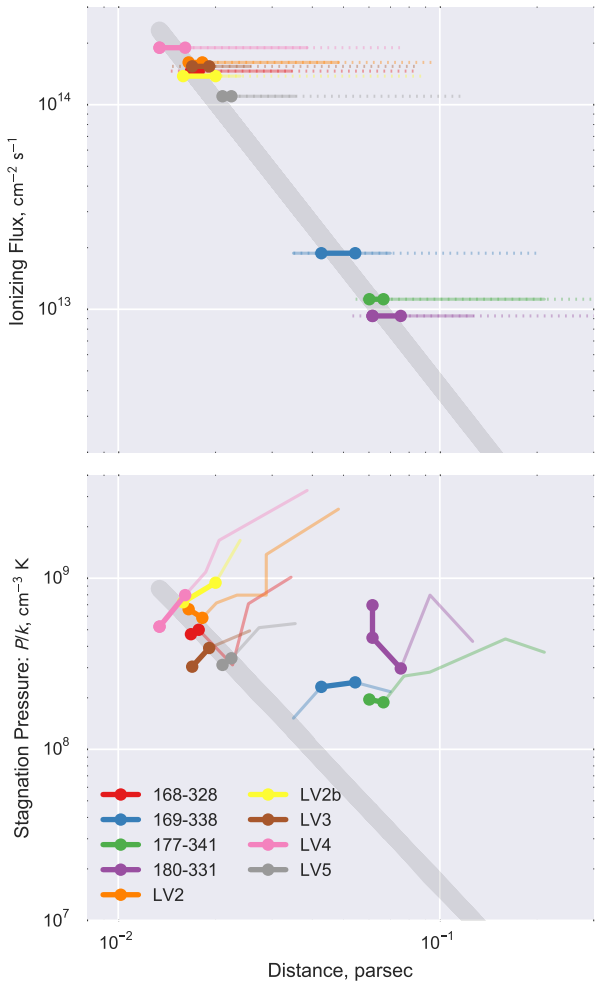

Figure 5. Top: In colored lines, we show the ionizing flux required to balance the photoevaporated flow for some models which agree with the observed radii for each proplyd compared against the stellar ionizing flux at the distance D. Bottom: The estimated stagnation pressure for the same models as above compared against the stellar wind pressure. In both graphs, the big dots represent th models which show agreement with ionization balance.